

Neutron-proton bremsstrahlung calculation: Noncoplanarity effects

Yi Li and M. K. Liou

Department of Physics and Institute for Nuclear Theory, Brooklyn College of the City University of New York, Brooklyn, New York 11210

W. M. Schreiber

Department of Physics, The College of Staten Island of the City University of New York, Staten Island, New York 10314

(Received 18 June 2001; published 21 November 2001)

Coplanar and noncoplanar $np\gamma$ cross sections and coplanar $np\gamma$ analyzing powers are calculated in the energy region between 130 and 200 MeV for various nucleon scattering angles. Both pseudoscalar and pseudovector πN couplings have been considered in our calculations. The results are used to investigate noncoplanarity effects. Agreement with available $np\gamma$ data is good for most cases, but discrepancies do exist for some data points. We show that the dependence of the noncoplanar cross sections upon the noncoplanarity angle is significantly different at different photon angles. This suggests that this more general approach should be used to investigate the important noncoplanarity effects. Similar to what has previously been observed in potential-model calculations, the meson-exchange effects dominate the $np\gamma$ process. To the best of our knowledge, results for $np\gamma$ analyzing powers have heretofore not been calculated. As far as we know, no $np\gamma$ analyzing power experimental data are presently available for comparison, but these results should prove useful for future experiments. The differences in either cross sections or analyzing powers calculated using the two couplings are very small for all cases studied, in contradistinction to our previous calculations for the $pp\gamma$ process where the differences were found to be greater.

DOI: 10.1103/PhysRevC.64.064002

PACS number(s): 25.40.-h, 13.40.-f, 13.75.Cs, 13.75.Gx

I. INTRODUCTION

Recently, we have applied both proton-proton bremsstrahlung ($pp\gamma$) and neutron-proton bremsstrahlung ($np\gamma$) processes to investigate an important problem related to the pion-nucleon coupling (πN coupling, $NN\pi$) [1]. Treating the πN coupling not only as pseudoscalar (ps) but also a pseudovector (pv), we have calculated both coplanar and noncoplanar cross sections in Ref. [1] using a realistic one-boson-exchange (OBE) model obtained by Horowitz [2]. Specifically, $pp\gamma$ and $np\gamma$ cross sections have been calculated with the ps coupling ($\sigma_{pp\gamma}^{ps}$ and $\sigma_{np\gamma}^{ps}$) and the pv coupling ($\sigma_{pp\gamma}^{pv}$ and $\sigma_{np\gamma}^{pv}$). From these cross sections, the deviation in the $pp\gamma$ cross section, $\Delta_{pp\gamma} \equiv \sigma_{pp\gamma}^{ps} - \sigma_{pp\gamma}^{pv}$, and the deviation in the $np\gamma$ cross section, $\Delta_{np\gamma} \equiv \sigma_{np\gamma}^{ps} - \sigma_{np\gamma}^{pv}$, can be determined. Even though the deviation $\Delta_{np\gamma}$ for the $np\gamma$ case is found to be too small to differentiate between the two couplings, the sensitive result for $\Delta_{pp\gamma}$ in some kinematic regions demonstrates that the $pp\gamma$ process could be used to study the ps - pv problem. Moreover, an encouraging finding is that $\Delta_{pp\gamma}$ increases dramatically if off-shell effects in the $p\gamma p$ vertex are taken into account. This fact implies that the investigation of the ps - pv problem should be combined with the study of the $p\gamma p$ vertex.

Using the $pp\gamma$ process, we have also performed another very thorough study of the ps - pv question and the on-shell vs off-shell $p\gamma p$ vertex problem [3]. In Ref. [3], we have developed an approach which can be applied to systematically investigate these two complex problems together. The most important conclusion obtained in Ref. [3] is that the experimental $pp\gamma$ data for both cross sections and analyzing powers in the energy region between 157 and 280 MeV can only be consistently described by the calculations using the

off-shell $p\gamma p$ vertex and the pv coupling. Indeed an important consequence of chiral symmetry is that pseudovector πN coupling is favored. In fact, the pion has been treated as a Goldstone boson associated with spontaneous symmetry breaking, which in turn implies pseudovector coupling [4].

In this work, we have focused on the $np\gamma$ process and calculated relevant cross sections and analyzing powers. As expected, the deviation $\Delta_{np\gamma}$ is indeed very small and does not shed any additional light on the difference between the two couplings. On the other hand, we have found that the dependence of the noncoplanar cross sections upon the noncoplanarity angle is significantly different at different photon angles. Thus the main purpose of this work is to investigate the noncoplanarity effects in $np\gamma$. The off-shell nucleon electromagnetic vertices ($p\gamma p$ and $n\gamma n$ vertices) have not been used in our $np\gamma$ calculations, primarily because the determination of the off-shell $n\gamma n$ vertex requires experimental $np\gamma$ analyzing powers as input in our approach, but such experimental data is currently not available, as far as we know. To be consistent, only on-shell $p\gamma p$ and $n\gamma n$ vertices have been used in this work.

The idea of using nucleon-nucleon bremsstrahlung as a tool for investigating the ps - pv problem is rather new. This idea has recently attracted considerable attention [1,3,5–7]. It has been pointed out [6] that the contribution from negative energy states may be significant to the problem in the $pp\gamma$ case. Our model does not naturally incorporate such contributions. For the $pp\gamma$ case, such investigations have been performed [7], and the contribution from negative energy states has been found to be small for photon energies less than 100 MeV. Furthermore, since exchange effects dominate $np\gamma$, it is likely that negative energy contributions will be small in this case.

Most of the nucleon-nucleon bremsstrahlung experiments

performed during the last three decades were $pp\gamma$ experiments. Very few $np\gamma$ cross sections (mostly at large scattering angles), and no analyzing powers, have been measured [8]. Generally speaking, the $np\gamma$ experiments are much more difficult to perform than the $pp\gamma$ experiments. In particular, detecting charged proton beams is easier than detecting neutral neutron beams, and the neutron beams lack the high quality and/or intensity required for precise measurements. Recently, the $np\gamma$ process has received renewed attention because the $np\gamma$ process appears to be the most likely source of energetic photons emitted from heavy-ion collisions [9], and it is probably an ideal process for studying meson-exchange effects [10].

A variety of models and approximations have been proposed during the past three decades for bremsstrahlung calculations. In studying the $pp\gamma$ and $np\gamma$ processes, most theoretical investigations have focused on nonrelativistic potential-model calculations using various phenomenological potentials as input. For the $np\gamma$ case, an important finding obtained from these nonrelativistic potential-model calculations is that meson-exchange currents are the dominant source of high energy photons. More precisely, Brown and Franklin [10] have calculated the $np\gamma$ cross section using the electromagnetic Hamiltonian, which includes the coupling of the electromagnetic field to the nucleon currents V_{em}^1 and the coupling of the electromagnetic field to the exchange currents V_{em}^2 . As a result, large exchange effects from V_{em}^2 were predicted. The inclusion of the V_{em}^2 term has been found to increase the $np\gamma$ cross section by about a factor of 2. This finding has been confirmed by Nakayama [11].

These exchange effects can also be observed even more directly from our one-boson-exchange approach, as will be discussed in Secs. II and III. A unique feature of our OBE approach is that the exchange effects have been explicitly taken into account in our calculations. Another important advantage of using the OBE model is that the constructed $np\gamma$ amplitudes are both Lorentz invariant and gauge invariant. Furthermore, the model allows us to readily incorporate both the ps coupling and the pv coupling.

The organization of this paper is as follows. The expression for the np elastic amplitude in Horowitz's model is given in Sec. II. In Sec. III, we describe the two different $np\gamma$ amplitudes, one for the ps coupling $M_{np\gamma,\mu}^{ps}$ and another for the pv coupling $M_{np\gamma,\mu}^{pv}$, which have been used in our calculations. In Sec. IV, our calculated results of (coplanar and noncoplanar) cross sections and analyzing powers are presented. The results are compared with the experimental data and other calculations using the potential model. In this section, significant noncoplanarity effects in $np\gamma$ are demonstrated. Implications of our results are discussed in the concluding section.

II. ELASTIC np AMPLITUDE

We consider photon emission accompanying the np scattering:

$$p(p_1^\mu) + n(p_2^\mu) \rightarrow p(p_3^\mu) + n(p_4^\mu) + \gamma(K^\mu). \quad (1)$$

The five four-momenta in Eq. (1) satisfy energy-momentum conservation,

$$p_1^\mu + p_2^\mu = p_3^\mu + p_4^\mu + K^\mu, \quad (2)$$

and they can be used to define the following Mandelstam variables:

$$\begin{aligned} s_{12} &= (p_1 + p_2)^2, & s_{34} &= (p_3 + p_4)^2, \\ t_{13} &= (p_1 - p_3)^2, & t_{24} &= (p_2 - p_4)^2, \\ u_{23} &= (p_2 - p_3)^2, & u_{14} &= (p_1 - p_4)^2. \end{aligned} \quad (3)$$

In the limit when K approaches zero, the $np\gamma$ process (1) reduces to the corresponding np elastic scattering process,

$$p(p_1^\mu) + n(p_2^\mu) \rightarrow p(\bar{p}_3^\mu) + n(\bar{p}_4^\mu), \quad (4)$$

where

$$\begin{aligned} \bar{p}_3^\mu &= \lim_{k \rightarrow 0} p_3^\mu, \\ \bar{p}_4^\mu &= \lim_{k \rightarrow 0} p_4^\mu. \end{aligned} \quad (5)$$

In this limit, Eqs. (2) and (3) become

$$\begin{aligned} p_1^\mu + p_2^\mu &= \bar{p}_3^\mu + \bar{p}_4^\mu, \\ s &= (p_1 + p_2)^2 = (\bar{p}_3 + \bar{p}_4)^2, \\ t &= (p_1 - \bar{p}_3)^2, & u &= (p_2 - \bar{p}_3)^2. \end{aligned} \quad (7)$$

In this work, we use Horowitz's OBE model [2,3] to obtain the $np\gamma$ amplitude. To construct the $np\gamma$ amplitude from Horowitz's model, we follow the procedure discussed in Ref. [3]. Specifically, instead of generating the $np\gamma$ amplitude from the five-term representation of the elastic np amplitude [2], we first construct Horowitz OBE diagrams for the elastic process and then attach the photon to these diagrams to obtain the $np\gamma$ amplitude. The elastic np amplitude corresponding to the OBE diagrams, valid for both ps and pv couplings, has the form

$$\begin{aligned} M_{np}(u, t) &= \sum_{\alpha=1}^5 \left\{ - \sum_{\beta=1}^2 [G_{\alpha\beta}(t) f_{\alpha\beta}^2(t) \bar{u}(\bar{p}_3, \nu_3) \lambda_\alpha \right. \\ &\quad \times u(p_1, \nu_1) \bar{u}(\bar{p}_4, \nu_4) \lambda^\alpha u(p_2, \nu_2) \\ &\quad + 2G_{\alpha\beta}(u) f_{\alpha\beta}^2(u) \bar{u}(\bar{p}_4, \nu_4) \lambda_\alpha u(p_1, \nu_1) \\ &\quad \times \bar{u}(\bar{p}_3, \nu_3) \lambda^\alpha u(p_2, \nu_2)] \\ &\quad + \sum_{\beta=3}^4 G_{\alpha\beta}(t) f_{\alpha\beta}^2(t) \bar{u}(\bar{p}_3, \nu_3) \lambda_\alpha u(p_1, \nu_1) \\ &\quad \times \bar{u}(\bar{p}_4, \nu_4) \lambda^\alpha u(p_2, \nu_2) \left. \right\}, \end{aligned} \quad (8)$$

where

$$(\lambda_1, \lambda_2, \lambda_3, \lambda_4, \lambda_5) \equiv (1, \sigma_{\mu\nu}, \gamma_5 \gamma_\mu, \gamma_\mu, \gamma_5), \quad (9a)$$

$$(\lambda^1, \lambda^2, \lambda^3, \lambda^4, \lambda^5) \equiv (1, \sigma^{\mu\nu}, \gamma_5 \gamma^\mu, \gamma^\mu, \gamma_5), \quad (9b)$$

$$f_{\alpha\beta}(x) = \frac{\Lambda_{\alpha\beta}^2}{x - \Lambda_{\alpha\beta}^2}, \quad (9c)$$

$$G_{\alpha\beta}(x) = 4\pi g_{\alpha\beta}^2 \frac{i}{x - m_{\alpha\beta}^2 + i\epsilon_{\alpha\beta}}, \quad x = t, u. \quad (9d)$$

The elastic cross sections calculated using the above amplitude $M_{np}(u, t)$ are identical to those obtained from Horowitz's amplitude in the five-term representation. The Horowitz parameters, which involve the complex coupling constants $g_{\alpha\beta}^2$, the cutoff parameters $\Lambda_{\alpha\beta}$, and the meson masses $m_{\alpha\beta}$, are defined in Appendix A of Ref. [3]. Note that $t = -q^2$ and $u = -Q^2$, where q and Q are, respectively, the direct momentum transfer and the exchange momentum transfer used by Horowitz [2].

III. $np\gamma$ AMPLITUDE

It is straightforward to generate $np\gamma$ diagrams from the np elastic diagrams in the OBE model. The $np\gamma$ amplitude can be easily obtained from the $np\gamma$ diagrams. As we have already mentioned in the introduction, only the on-shell neutron electromagnetic vertex will be used in the $np\gamma$ amplitude. The main reason is that the off-shell $n\gamma n$ vertex cannot be determined in our approach without the experimental $np\gamma$ analyzing power data, but to the best of our knowledge, such data is not currently available. As for the proton electromagnetic vertex, we can use either the on-shell or the off-shell $p\gamma p$ vertices. However, because the exchange effects (the internal contribution) dominate the $np\gamma$ cross section, the difference between the results obtained from the on-shell and the off-shell $p\gamma p$ vertices is expected to be small. For consistency, we have also used the on-shell $p\gamma p$ vertex for all $np\gamma$ calculations.

For ps coupling, the $np\gamma$ amplitude has the form

$$\begin{aligned} M_{np\gamma, \mu}^{ps} = & i \sum_{\alpha=1}^5 \left\{ - \sum_{\beta=1}^2 \left[G_{\alpha\beta}(t_{24}) f_{\alpha\beta}^2(t_{24}) \bar{u}(p_3, \nu_3) X_{\alpha\mu} u(p_1, \nu_1) \bar{u}(p_4, \nu_4) \lambda^\alpha u(p_2, \nu_2) + G_{\alpha\beta}(t_{13}) \right. \right. \\ & \times f_{\alpha\beta}^2(t_{13}) \bar{u}(p_3, \nu_3) \lambda_\alpha u(p_1, \nu_1) \bar{u}(p_4, \nu_4) \tilde{Y}_\mu^\alpha u(p_2, \nu_2) + 2G_{\alpha\beta}(u_{14}) f_{\alpha\beta}^2(u_{14}) \bar{u}(p_4, \nu_4) \lambda_\alpha u(p_1, \nu_1) \\ & \times \bar{u}(p_3, \nu_3) \tilde{Z}_\mu^\alpha u(p_2, \nu_2) + 2G_{\alpha\beta}(u_{23}) f_{\alpha\beta}^2(u_{23}) \bar{u}(p_4, \nu_4) \tilde{T}_{\alpha\mu} u(p_1, \nu_1) \bar{u}(p_3, \nu_3) \lambda^\alpha u(p_2, \nu_2) \\ & + 2G_{\alpha\beta}(u_{14}) f_{\alpha\beta}(u_{14}) f_{\alpha\beta}(u_{23}) \left(1 + \frac{u_{14} - m_{\alpha\beta}^2}{u_{23} - \Lambda_{\alpha\beta}^2} + \frac{u_{23} - m_{\alpha\beta}^2}{u_{14} - \Lambda_{\alpha\beta}^2} \right) \frac{(p_1 + p_3 - p_2 - p_4)_\mu}{u_{23} - m_{\alpha\beta}^2 + i\epsilon_{\alpha\beta}} \\ & \times \bar{u}(p_4, \nu_4) \lambda_\alpha u(p_1, \nu_1) \bar{u}(p_3, \nu_3) \lambda^\alpha u(p_2, \nu_2) \left. \right] + \sum_{\beta=3}^4 [G_{\alpha\beta}(t_{24}) f_{\alpha\beta}^2(t_{24}) \bar{u}(p_3, \nu_3) X_{\alpha\mu} \\ & \times u(p_1, \nu_1) \bar{u}(p_4, \nu_4) \lambda^\alpha u(p_2, \nu_2) + G_{\alpha\beta}(t_{13}) f_{\alpha\beta}^2(t_{13}) \bar{u}(p_3, \nu_3) \lambda_\alpha u(p_1, \nu_1) \\ & \times \bar{u}(p_4, \nu_4) \tilde{Y}_\mu^\alpha u(p_2, \nu_2)] \left. \right\}, \end{aligned} \quad (10)$$

where

$$\begin{aligned} X_{\alpha\mu} = & \lambda_\alpha \frac{1}{\not{p}_1 - \not{K} - m + i\epsilon} \Gamma_\mu^p + \Gamma_\mu^p \frac{1}{\not{p}_3 + \not{K} - m + i\epsilon} \lambda_\alpha, \\ \tilde{Y}_\mu^\alpha = & \lambda^\alpha \frac{1}{\not{p}_2 - \not{K} - m + i\epsilon} \Gamma_\mu^n + \Gamma_\mu^n \frac{1}{\not{p}_4 + \not{K} - m + i\epsilon} \lambda^\alpha, \end{aligned} \quad (11a)$$

$$\begin{aligned} \tilde{Z}_\mu^\alpha = & \lambda^\alpha \frac{1}{\not{p}_2 - \not{K} - m + i\epsilon} \Gamma_\mu^n + \Gamma_\mu^p \frac{1}{\not{p}_3 + \not{K} - m + i\epsilon} \lambda^\alpha, \\ \tilde{T}_{\alpha\mu} = & \lambda_\alpha \frac{1}{\not{p}_1 - \not{K} - m + i\epsilon} \Gamma_\mu^p + \Gamma_\mu^n \frac{1}{\not{p}_4 + \not{K} - m + i\epsilon} \lambda_\alpha, \end{aligned} \quad (11b)$$

and the following on-shell nucleon electromagnetic vertices have been used:

$$\Gamma_\mu^p = \gamma_\mu - \frac{i\kappa_p}{2m} \sigma_{\mu\nu} K^\nu, \quad \kappa_p = 1.79, \quad (12)$$

$$\Gamma_\mu^n = -i \frac{\kappa_n}{2m} \sigma_{\mu\nu} K^\nu, \quad \kappa_n = -1.91. \quad (13)$$

Those terms involving the factors ([12])

$$f_{\alpha\beta}(u_{14}) f_{\alpha\beta}(u_{23}) \left(1 + \frac{u_{14} - m_{\alpha\beta}^2}{u_{23} - \Lambda_{\alpha\beta}^2} + \frac{u_{23} - m_{\alpha\beta}^2}{u_{14} - \Lambda_{\alpha\beta}^2} \right) \quad (14)$$

in Eq. (10) belong to the internal amplitude. This internal amplitude can be obtained from the external amplitude by imposing the condition for gauge invariance. The extra terms that depend on u_{14} and u_{23} in Eq. (14) are required for current conservation. These terms arise from the fact that the phenomenological form factors shown in Eq. (9c) have been introduced in Horowitz's model.

For pv coupling, the expression for the $np\gamma$ amplitude is

$$\begin{aligned}
 M_{np\gamma,\mu}^{pv} = & M_{np\gamma,\mu}^{ps} - \sum_{\beta=1}^2 \left[G_{5\beta}(t_{24})f_{5\beta}^2(t_{24})\bar{u}(p_3, \nu_3)(X'_{5\mu} - X_{5\mu})u(p_1, \nu_1)\bar{u}(p_4, \nu_4)\lambda^5 u(p_2, \nu_2) \right. \\
 & + G_{5\beta}(t_{13})f_{5\beta}^2(t_{13})\bar{u}(p_3, \nu_3)\lambda^5 u(p_1, \nu_1)\bar{u}(p_4, \nu_4)(\tilde{Y}'_{\mu}{}^5 - \tilde{Y}_{\mu}^5)u(p_2, \nu_2) + 2G_{5\beta}(u_{14})f_{5\beta}^2(u_{14}) \\
 & \times \bar{u}(p_4, \nu_4)\lambda^5 u(p_1, \nu_1)\bar{u}(p_3, \nu_3)(\tilde{Z}'_{\mu}{}^5 - \tilde{Z}_{\mu}^5)u(p_2, \nu_2) + 2G_{5\beta}(u_{23})f_{5\beta}^2(u_{23})\bar{u}(p_4, \nu_4) \\
 & \times (\tilde{T}'_{5\mu} - \tilde{T}_{5\mu})u(p_1, \nu_1)\bar{u}(p_3, \nu_3)\lambda^5 u(p_2, \nu_2) - G_{5\beta}(u_{23})f_{5\beta}^2(u_{23})\frac{1}{m}\bar{u}(p_4, \nu_4)\lambda_5 \gamma_{\mu} u(p_1, \nu_1) \\
 & \left. \times \bar{u}(p_3, \nu_3)\lambda^5 u(p_2, \nu_2) - G_{5\beta}(u_{14})f_{5\beta}^2(u_{14})\frac{1}{m}\bar{u}(p_4, \nu_4)\lambda_5 u(p_1, \nu_1)\bar{u}(p_3, \nu_3)\gamma_{\mu}\lambda^5 u(p_2, \nu_2) \right], \quad (15)
 \end{aligned}$$

where

$$\begin{aligned}
 X'_{5\mu} = & \left(\lambda^5 \frac{p_1 - p_3 - K}{2m} \right) \frac{1}{p_1 - K - m + i\epsilon} \Gamma_{\mu}^p \\
 & + \Gamma_{\mu}^p \frac{1}{p_3 + K - m + i\epsilon} \left(\lambda^5 \frac{p_1 - p_3 - K}{2m} \right), \\
 \tilde{Y}'_{\mu}{}^5 = & \left(\lambda^5 \frac{p_2 - p_4 - K}{2m} \right) \frac{1}{p_2 - K - m + i\epsilon} \Gamma_{\mu}^n \\
 & + \Gamma_{\mu}^n \frac{1}{p_4 + K - m + i\epsilon} \left(\lambda^5 \frac{p_2 - p_4 - K}{2m} \right), \\
 \tilde{Z}'_{\mu}{}^5 = & \left(\lambda^5 \frac{p_2 - p_3 - K}{2m} \right) \frac{1}{p_2 - K - m + i\epsilon} \Gamma_{\mu}^n \\
 & + \Gamma_{\mu}^p \frac{1}{p_3 + K - m + i\epsilon} \left(\lambda^5 \frac{p_2 - p_3 - K}{2m} \right), \\
 \tilde{T}'_{5\mu} = & \left(\lambda^5 \frac{p_1 - p_4 - K}{2m} \right) \frac{1}{p_1 - K - m + i\epsilon} \Gamma_{\mu}^p \\
 & + \Gamma_{\mu}^n \frac{1}{p_4 + K - m + i\epsilon} \left(\lambda^5 \frac{p_1 - p_4 - K}{2m} \right). \quad (16)
 \end{aligned}$$

Note that the amplitude $M_{np\gamma,\mu}^{pv}$ takes into account photon emissions from πN vertices.

Clearly, the two amplitudes $M_{np\gamma,\mu}^{ps}$ and $M_{np\gamma,\mu}^{pv}$ depend only upon relativistic invariants and they are fully gauge invariant. They have been used to calculate the noncoplanar differential cross sections $\sigma_{np\gamma}^{ps} (\equiv d^3\sigma_{np\gamma}^{ps}/d\Omega_3 d\Omega_4 d\psi_{\gamma})$ and $\sigma_{np\gamma}^{pv} (\equiv d^3\sigma_{np\gamma}^{pv}/d\Omega_3 d\Omega_4 d\psi_{\gamma})$, as a function of the photon angle ψ_{γ} and the noncoplanarity angle $\bar{\phi}$ ($\bar{\phi}=0$ gives

the coplanar cross section). We have also integrated the differential cross sections over ψ_{γ} to obtain the integrated cross sections as a function of $\bar{\phi}$,

$$d^2\sigma_{np\gamma}^{ps(pv)}/d\Omega_3 d\Omega_4 = \int (d^3\sigma_{np\gamma}^{ps(pv)}/d\Omega_3 d\Omega_4 d\psi_{\gamma}) d\psi_{\gamma}.$$

In the past, the curve that represents the integrated cross sections as a function of $\bar{\phi}$ has been used to investigate noncoplanarity effects in $np\gamma$. In fact, this curve allows one to obtain a constant correction factor C that can be used to convert the experimental noncoplanar cross sections to experimental coplanar cross sections [13]. Obviously, this factor is independent of ψ_{γ} . However, as discussed in Ref. [13], the noncoplanarity effect should be investigated more pre-

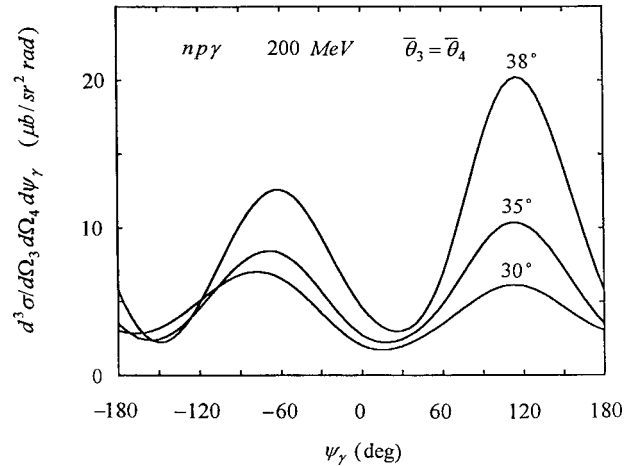


FIG. 1. Coplanar $np\gamma$ cross sections $\sigma_{np\gamma}^{pv}$ as functions of ψ_{γ} at 200 MeV for $\bar{\theta}_3 = \bar{\theta}_4 = 30^\circ, 35^\circ$, and 38° . The cross sections $\sigma_{np\gamma}^{ps}$ are not shown in this figure mainly because they are very close to the cross sections $\sigma_{np\gamma}^{pv}$.

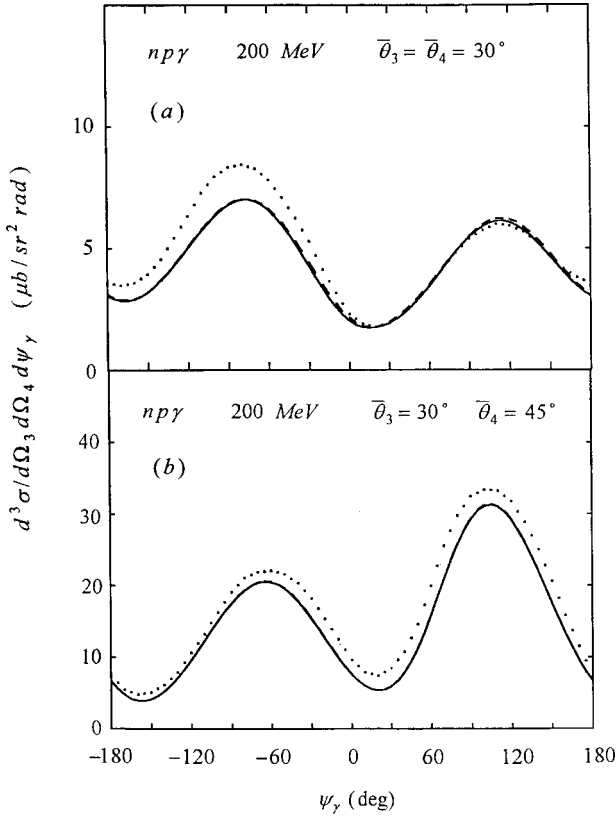


FIG. 2. (a) Coplanar $np\gamma$ cross sections as functions of ψ_γ at 200 MeV for $\bar{\theta}_3 = \bar{\theta}_4 = 30^\circ$. Our cross sections, $\sigma_{np\gamma}^{pv}$ (solid curve) and $\sigma_{np\gamma}^{ps}$ (dashed curve), are compared with the potential-model predictions (dotted curve) obtained by Brown and Franklin (Ref. [10]). (b) Coplanar $np\gamma$ cross sections as functions of ψ_γ at 200 MeV for $\bar{\theta}_3 = 30^\circ$ and $\bar{\theta}_4 = 45^\circ$. Our cross sections, $\sigma_{np\gamma}^{pv}$ (solid curve) and $\sigma_{np\gamma}^{ps}$ (dashed curve), are compared with the potential-model predictions (dotted curve) obtained by Herrmann, Speth, and Nakayama (Ref. [14]).

cisely as to the dependence of $d^3\sigma/d\Omega_3 d\Omega_4 d\psi_\gamma$ upon $\bar{\phi}$ at different photon angles ψ_γ . Thus, the standard noncoplanar curve should be $\sigma_{np\gamma}^{ps}$ (or $\sigma_{np\gamma}^{pv}$) as a function of $\bar{\phi}$ for a given angle ψ_γ . For this reason, the standard noncoplanar curves have also been calculated. They can be used to estimate ψ_γ -dependent correction factors $C(\psi_\gamma)$ [13]. Finally, we have also calculated analyzing powers A_y^{ps} and A_y^{pv} .

IV. RESULTS AND DISCUSSION

We have calculated $np\gamma$ coplanar and noncoplanar cross sections, $\sigma_{np\gamma}^{ps}$ for ps coupling and $\sigma_{np\gamma}^{pv}$ for pv coupling, and $np\gamma$ analyzing powers A_y^{ps} and A_y^{pv} . The relevant formulas used in these calculations can be found in Appendix C of Ref. [3]. Some results at 200 and 130 MeV are shown in Figs. 1–9. These results are compared with the experimental data and the results calculated using other approaches. Although not explicitly shown, contributions due to bremsstrahlung emissions from the exchange of charged mesons are found to dominate both cross sections and analyzing powers.

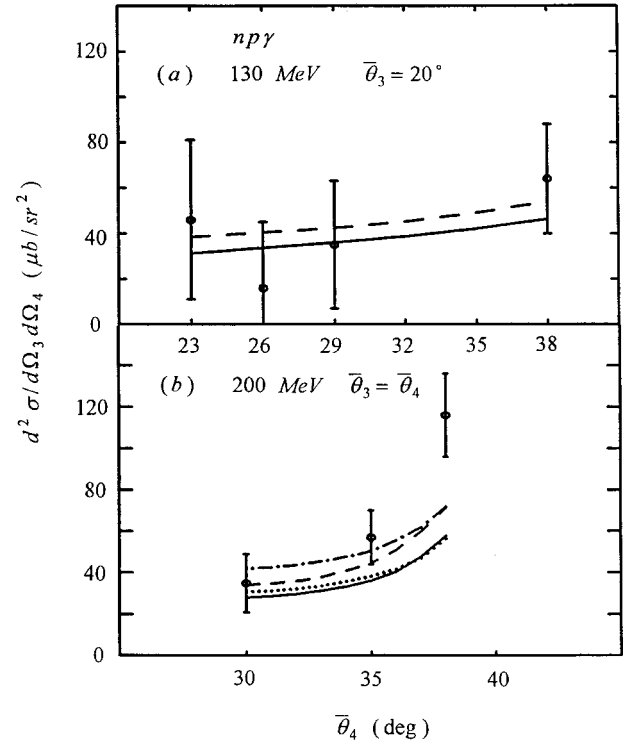


FIG. 3. (a) Integrated $np\gamma$ cross sections as functions of $\bar{\theta}_4$ at 130 MeV for $\bar{\theta}_3 = 20^\circ$. Our calculation $d^2\sigma_{np\gamma}^{pv}/d\Omega_3 d\Omega_4$ (solid curve) is compared with the potential-model result (dashed curve) obtained by Brown and Franklin (Ref. [10]). The experimental data are from Ref. [15]. (b) Integrated $np\gamma$ cross sections as functions of the symmetric scattering angles ($\bar{\theta}_3 = \bar{\theta}_4$) at 200 MeV. Our result $d^2\sigma_{np\gamma}^{pv}/d\Omega_3 d\Omega_4$ (solid curve) is compared with the results obtained by Brown and Franklin (Ref. [10]) (dashed curve), Herrmann, Speth, and Nakayama (Ref. [14]) (dotted curve), and Schäfer *et al.* (Ref. [17]) (dash-dotted curve). The experimental data are from Ref. [16].

In Fig. 1, we present the coplanar cross section $\sigma_{np\gamma}^{pv}$ as a function of ψ_γ ($-180^\circ \leq \psi_\gamma \leq 180^\circ$) at 200 MeV for $\bar{\theta}_3 = \bar{\theta}_4 = 30^\circ, 35^\circ$, and 38° . The cross sections $\sigma_{np\gamma}^{ps}$, which are very close to $\sigma_{np\gamma}^{pv}$ for all cases, are not shown in this figure. Because the deviation $\Delta_{np\gamma} = \sigma_{np\gamma}^{ps} - \sigma_{np\gamma}^{pv}$ is extremely small, the $np\gamma$ process at this energy and these angles cannot be used to distinguish between the ps and pv couplings. Note that the cross section $\sigma_{np\gamma}^{pv}$ increases as the symmetric scattering angle $\bar{\theta}_3 = \bar{\theta}_4$ increases in the range $-100^\circ \leq \psi_\gamma \leq 180^\circ$.

In Fig. 2, we compare our results with two well-known potential-model calculations. In Fig. 2(a), our calculated cross sections, $\sigma_{np\gamma}^{pv}$ (solid curve) and $\sigma_{np\gamma}^{ps}$ (dashed curve) at 200 MeV for $\bar{\theta}_3 = \bar{\theta}_4 = 30^\circ$, are compared with the cross sections calculated by Brown and Franklin (dotted curve) [10]. The agreement between the two calculations is extremely good for the second peak ($0^\circ \leq \psi_\gamma \leq 180^\circ$), but our first peak ($-180^\circ \leq \psi_\gamma \leq 0^\circ$) is about 20%–30% smaller than their peak. In Fig. 2(b), our calculated cross sections [$\sigma_{np\gamma}^{pv}$ (solid curve) and $\sigma_{np\gamma}^{ps}$ (dashed curve) are too close to be distinguished] at 200 MeV for $\bar{\theta}_3 = 30^\circ$ and $\bar{\theta}_4 = 45^\circ$ are compared

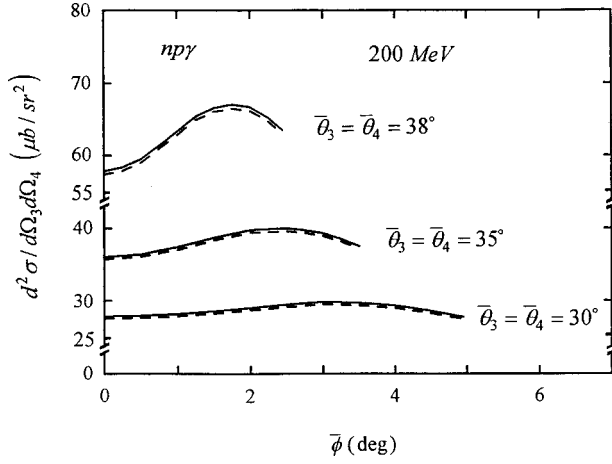


FIG. 4. Integrated $np\gamma$ cross section $d^2\sigma_{np\gamma}^{pv(ps)}/d\Omega_3d\Omega_4$ as a function of $\bar{\phi}$ at 200 MeV for $\bar{\theta}_3 = \bar{\theta}_4 = 30^\circ, 35^\circ$, and 38° . The solid and dashed curves represent the results for the ps and pv couplings, respectively.

with the cross section calculated by Herrmann, Speth, and Nakayama (dotted curve) [14]. Agreement between the results calculated using the two different approaches is very good.

In Fig. 3(a), we show integrated cross sections

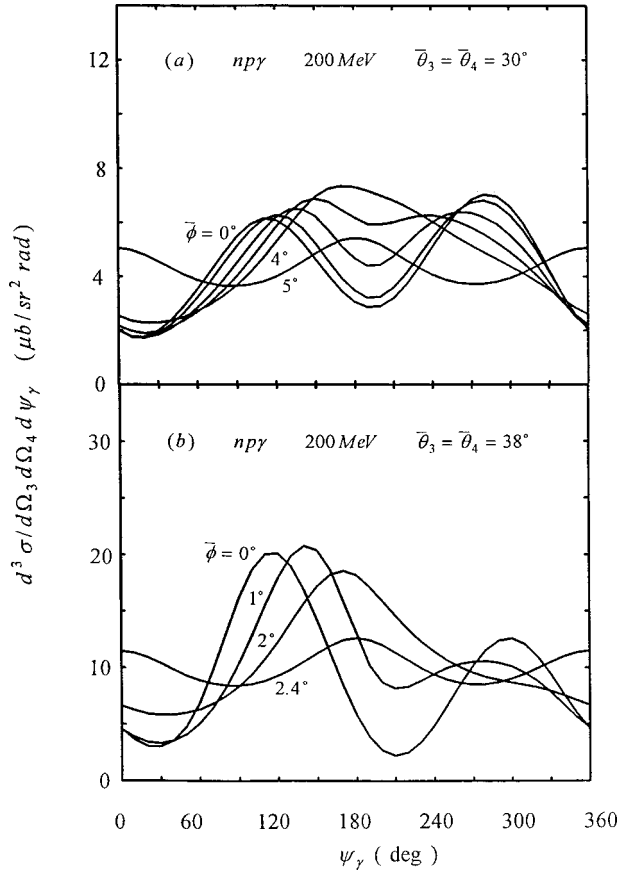


FIG. 5. Noncoplanar $np\gamma$ cross sections $\sigma_{np\gamma}^{pv}$ as functions of ψ_γ at 200 MeV for several noncoplanarity angles $\bar{\phi}$: (a) $\bar{\theta}_3 = \bar{\theta}_4 = 30^\circ$ and (b) $\bar{\theta}_3 = \bar{\theta}_4 = 38^\circ$.

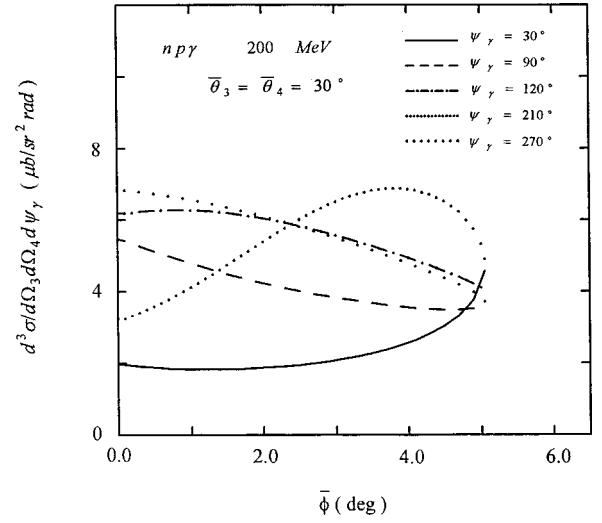
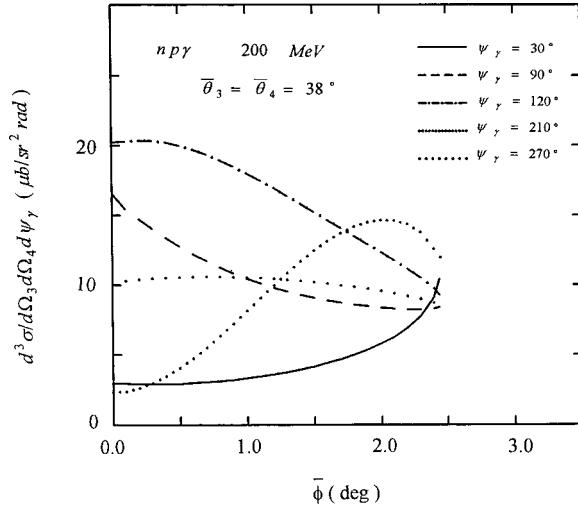


FIG. 6. Noncoplanar $np\gamma$ cross sections $\sigma_{np\gamma}^{pv}$ as a function of $\bar{\phi}$ for a given $\psi_\gamma (= 30^\circ, 90^\circ, 120^\circ, 210^\circ, 270^\circ)$ at 200 MeV for $\bar{\theta}_3 = \bar{\theta}_4 = 30^\circ$.

$d^2\sigma_{np\gamma}^{pv}/d\Omega_3d\Omega_4$ as a function of $\bar{\theta}_4$ at 130 MeV for a fixed angle $\bar{\theta}_3 = 20^\circ$. Our result (solid curve) is compared with the experimental measurements [15] and the potential-model prediction of Brown and Franklin (dashed curve) [10]. All calculations are in good agreement with the experimental data. In Fig. 3(b), we show the integrated $np\gamma$ cross section at 200 MeV for several symmetric scattering angles, $\bar{\theta}_3 = \bar{\theta}_4 = 30^\circ, 35^\circ$ and 38° . Our result (solid curve) is compared with the experimental data [16] and three other calculations, i.e., by Brown and Franklin (dashed curve) [10], Herrmann, Speth, and Nakayama (dotted curve) [14], and Schäfer *et al.* (dash-dotted curve) [17]. Our result is in very close agreement with that of Herrmann, Speth, and Nakayama. The agreement between all calculations and the experimental data is good for $\bar{\theta}_3 = \bar{\theta}_4 = 30^\circ$, but poor for $\bar{\theta}_3 = \bar{\theta}_4 = 38^\circ$. The data for the 38° case is much greater than all theoretical predictions. As discussed below, it is likely that the noncoplanar effect is responsible for this large discrepancy between theory and experiment.

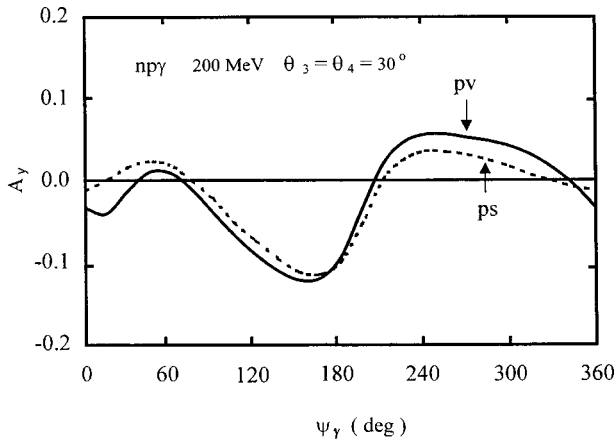
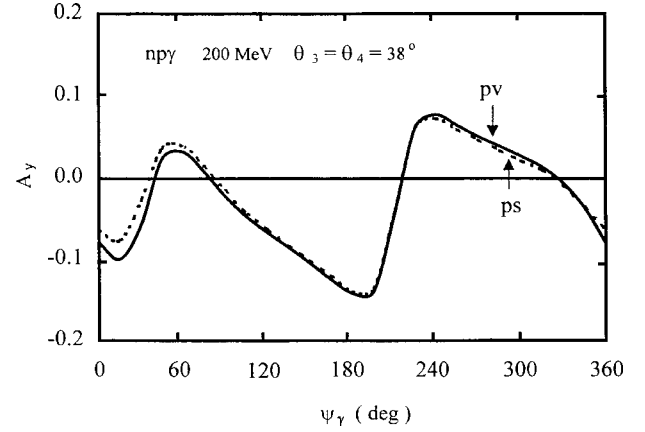
In Fig. 4, we present the integrated cross section $d^2\sigma_{np\gamma}^{pv(ps)}/d\Omega_3d\Omega_4$ as a function of the noncoplanarity angle $\bar{\phi}$ at 200 MeV for $\bar{\theta}_3 = \bar{\theta}_4 = 30^\circ, 35^\circ$, and 38° . Some interesting features can be observed [1]. (i) The deviation $\Delta'_{np\gamma} (\equiv d^2\sigma_{np\gamma}^{ps}/d\Omega_3d\Omega_4 - d^2\sigma_{np\gamma}^{pv}/d\Omega_3d\Omega_4)$ is extremely small for all cases, suggesting that the $np\gamma$ process at 200 MeV and large scattering angles cannot be used to resolve the ps - pv problem. (ii) The general shape of the $np\gamma$ noncoplanar curves shown in this figure is quite different from that of the $pp\gamma$ noncoplanar curves (see Fig. 2 of Ref. [1] and Fig. 6 of Ref. [3]). These curves indicate that the experimentally detected bremsstrahlung events must be corrected in order to determine the true coplanar cross sections, and the correction factor C for the $np\gamma$ case should be quite different from that for the $pp\gamma$ case. (iii) Noncoplanarity effects increase as the symmetric scattering angles increase. The correction factor C for the three cases will be very different. The factor C for a

FIG. 7. Same as Fig. 6, but for $\bar{\theta}_3 = \bar{\theta}_4 = 38^\circ$.

small symmetric angle should be close to 1. The noncoplanarity effects for the 38° case is very significant, suggesting that such effects may explain the large discrepancy between theory and experiment.

In Fig. 5, we show noncoplanar $np\gamma$ cross sections $\sigma_{np\gamma}^{pv}$ as functions of Ψ_γ at 200 MeV for several noncoplanarity angles $\bar{\phi}$. These results demonstrate that the noncoplanarity effects, i.e., the dependence of $\sigma_{np\gamma}^{pv}$ upon $\bar{\phi}$, differ markedly as functions of Ψ_γ . Because of this significant angular dependence of the noncoplanarity, the noncoplanar cross section as a function of $\bar{\phi}$ for a given Ψ_γ , rather than the integrated cross section as a function of $\bar{\phi}$, should be used by experimentalists for converting the experimental (noncoplanar) cross section into a coplanar result. In other words, the correction factor $C(\Psi_\gamma)$, rather than the correction factor C , should be used.

In Fig. 6, we plot various standard noncoplanar curves for $\bar{\theta}_3 = \bar{\theta}_4 = 30^\circ$ at the incident energy 200 MeV. Each curve represents the noncoplanar cross section as a function of $\bar{\phi}$ for a given Ψ_γ . These noncoplanar curves show quite sig-

FIG. 8. Coplanar $np\gamma$ analyzing power at 200 MeV for $\bar{\theta}_3 = \bar{\theta}_4 = 30^\circ$.FIG. 9. Same as Fig. 8, but for $\bar{\theta}_3 = \bar{\theta}_4 = 38^\circ$.

nificant noncoplanarity effects that depend very much on Ψ_γ . In other words, the correction factors $C(\Psi_\gamma)$ obtained from these curves will be completely different at different Ψ_γ . Similar standard noncoplanar curves, but for $\bar{\theta}_3 = \bar{\theta}_4 = 38^\circ$, are given in Fig. 7.

Two sets of calculated $np\gamma$ analyzing powers at 200 MeV are shown in Fig. 8 for $\bar{\theta}_3 = \bar{\theta}_4 = 30^\circ$ and in Fig. 9 for $\bar{\theta}_3 = \bar{\theta}_4 = 38^\circ$. The deviation, $\Delta A \equiv A_\gamma^{ps} - A_\gamma^{pv}$, is larger for the 30° case than for the 38° case. However, it is still too small for an experiment to differentiate between the two couplings.

Finally, in order to estimate the contribution from the off-shell proton electromagnetic vertex (off-shell $p\gamma p$ vertex), we have also calculated both $np\gamma$ cross sections and analyzing powers at 200 MeV for $\bar{\theta}_3 = \bar{\theta}_4 = 20^\circ, 30^\circ, 35^\circ$, and 38° using the off-shell $p\gamma p$ and the on-shell $n\gamma n$ vertices in the calculations. The results of these calculations were compared with those using on-shell electromagnetic vertices for both the proton and the neutron. In general, the effect of the off-shell $p\gamma p$ vertex is small. We have found that the effect increases as the scattering angle decreases, and it can be completely ignored for the large scattering angles ($\bar{\theta}_3 = \bar{\theta}_4 > 35^\circ$).

V. CONCLUSION

We have calculated $np\gamma$ cross sections for both coplanar and noncoplanar cases, and $np\gamma$ analyzing powers for the coplanar case. Both pseudoscalar and pseudovector πN couplings have been considered. The results of our calculations have been used to investigate noncoplanarity effects.

The calculations based on the two different couplings (ps and pv) yield very similar results, where the $np\gamma$ analyzing powers are found to be slightly more sensitive to the difference between the two couplings in comparison with the $np\gamma$ cross sections. Our study confirms what has previously been observed in potential-model calculations that exchange effects dominate the $np\gamma$ process.

We have found that the dependence of the noncoplanar cross sections upon the noncoplanarity angle $\bar{\phi}$ is significantly different at different photon angles Ψ_γ . This in turn implies that this variation with Ψ_γ should be taken into ac-

count in the determination of the appropriate correction factors needed to yield the coplanar cross sections. It is most likely that the noncoplanar effect is responsible for some existing large discrepancy between theory and experiment.

The calculated $np\gamma$ analyzing powers have to the best of our knowledge heretofore not been done. Though experimental data on analyzing powers, as far as we know, is presently

not available, these calculations should prove useful for future experimentation in this area.

ACKNOWLEDGMENT

The work of M.K.L. and W.M.S. was supported in part by the City University of New York Professional Staff Congress, Board of Higher Education Research Award Program.

-
- [1] M. K. Liou, Yi Li, W. M. Schreiber, and R. W. Brown, Phys. Rev. C **52**, R2346 (1995).
 - [2] C. J. Horowitz, Phys. Rev. C **31**, 1340 (1985).
 - [3] Yi Li, M. K. Liou, and W. M. Schreiber, Phys. Rev. C **57**, 507 (1998).
 - [4] See, e.g., G. Baym and D. K. Campbell, in *Mesons in Nuclei*, edited by M. Rho and D. Wilkinson (North-Holland, Amsterdam, 1979), Chap. 27, and references therein.
 - [5] J. A. Eden and M. F. Gari, Phys. Rev. C **53**, 1102 (1996).
 - [6] F. de Jong and K. Nakayama, Phys. Lett. B **385**, 33 (1996).
 - [7] G. H. Martinus, O. Scholton, and J. A. Tjon, Phys. Rev. C **56**, 2945 (1997).
 - [8] For early references, see F. Malek, H. Nifenecker, J. A. Pinston, F. Schussler, S. Drissi, and J. Julien, Phys. Lett. B **266**, 255 (1991), and references therein. Ongoing experiments at the Los Alamos Neutron Science Center should produce additional data in the near future.
 - [9] H. Nifenecher and J. A. Pinston, Annu. Rev. Nucl. Part. Sci. **40**, 113 (1990), and references therein.
 - [10] V. R. Brown and J. Franklin, Phys. Rev. C **8**, 1706 (1973).
 - [11] K. Nakayama, Phys. Rev. C **39**, 1475 (1989).
 - [12] I. S. Towner, Phys. Rep. **155**, 263 (1987).
 - [13] Yi Li, M. K. Liou, R. Timmermans, and B. F. Gibson, Phys. Rev. C **58**, R1880 (1998).
 - [14] V. Herrmann, J. Speth, and K. Nakayama, Phys. Rev. C **43**, 394 (1991).
 - [15] J. A. Edgington, V. J. Howard, I. M. Blair, B. E. Bonner, F. P. Brady, and M. W. McNaughton, Nucl. Phys. A **218**, 151 (1974).
 - [16] F. P. Brady and J. C. Young, Phys. Rev. C **2**, 1579 (1970).
 - [17] M. Schäfer, T. S. Biro, W. Cassing, W. Mosel, H. Nifenecker, and J. A. Pinston, Z. Phys. A **339**, 391 (1991).